Article

Electron Transport by Molecular Motion of redox-DNA Strands: Unexpectedly Slow Rotational Dynamics of 20-mer ds-DNA Chains End-Grafted onto Surfaces via C Linkers

Agne#s Anne, and Christophe Demaille

J. Am. Chem. Soc., **2008**, 130 (30), 9812-9823 • DOI: 10.1021/ja801074m • Publication Date (Web): 02 July 2008

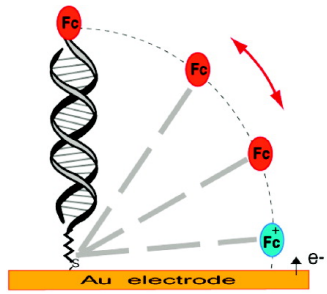

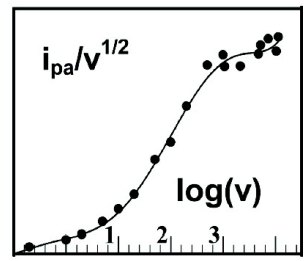

More About This Article

Additional resources and features associated with this article are available within the HTML version:

- Supporting Information
- Access to high resolution figures
- Links to articles and content related to this article
- Copyright permission to reproduce figures and/or text from this article

View the Full Text HTML

J|A|C|S
ARTICLES

Published on Web 07/02/2008

Electron Transport by Molecular Motion of redox-DNA Strands: Unexpectedly Slow Rotational Dynamics of 20-mer ds-DNA Chains End-Grafted onto Surfaces via C_6 Linkers

Agnès Anne and Christophe Demaille*

Laboratoire d'Electrochimie Moléculaire, Unité Mixte de Recherche Université - CNRS No. 7591, Université de Paris 7 - Denis Diderot, 2 place Jussieu, 75251 Paris Cedex 5, France

Received February 12, 2008; E-mail: demaille@paris7.jussieu.fr

Abstract: The dynamics of electron transport within molecular layers of 3′-ferrocenylated 20-mer oligonucleotide, 5′-thiol end-grafted onto gold electrode surfaces via a six-carbon (C_6) linker, is studied by cyclic voltammetry. Single-stranded Fc-DNA layers are observed to behave as diffusionless systems reflecting the rapid dynamics of the ssDNA strand. Following hybridization, the Fc-dsDNA-C_6 layers give rise to a characteristic cyclic voltammetry behavior evidencing that the Fc head is animated by a purely diffusional motion, which is ascribed to free rotation of the rigid DNA duplex around its C_6 anchoring linker. A model, describing the motion of the Fc head as resulting from hinge motion of the DNA duplex, is developed allowing the motional dynamics of the Fc-dsDNA-C_6 chains to be quantified in terms of an apparent rotational diffusion coefficient, D_r. The value found for D_r is ~3−4 orders of magnitude slower than expected for free rotation of dsDNA in solution, pointing to a drastic motion-slowing role of the anchoring surface. Accessibility of the Fc head for the electron transfer at the electrode is also shown to modulate the apparent dsDNA dynamics. The dynamics of Fc-dsDNA-C_6 is found to be insensitive to the presence of a single mismatch in the middle of the strand, confirming that charge transport by dsDNA conduction (DNA CT) is not present for the systems studied here. However, electron transport by free hinge motion of the dsDNA chain is shown to be fast enough to, *a priori*, compete favorably with DNA CT.

1. Introduction

The physical process responsible for charge transport within molecular layers of double-stranded (ds) DNA chains, end-anchored onto electrode surfaces and bearing a redox label at their free end, is still actively debated. DNA-mediated charge transport (DNA CT), an attractive phenomenon well-characterized in solution,[1] was initially thought to be the major, or even the sole, mechanism responsible for charge transport within these layers.[2] However, in previous works,[3,4] we showed that the dynamics of electron transport within a molecular monolayer of hybridized 3′-ferrocenylated-$(dT)_{20}$ oligonucleotides, 5′-thiol end-grafted onto gold electrode surfaces via a short two-carbon (C_2) alkyl linker (Fc-DNA-C_2 system, **III** in Chart 1), was actually controlled by the elastic bending of the redox-DNA duplex toward the electrode surface.

This was the first demonstration that molecular motion of the whole redox double-stranded (ds) DNA strand, allowing direct contact of the redox label with the electrode surface is, in itself, a very efficient charge transport mechanism. These initial reports triggered a recent reexamination of the contribution of DNA CT to the electrochemical response of end-anchored layers of redox-dsDNA.[5] In this later work Barton et

Chart 1. Chemical Structure of the 3′-Fc-Labeled Oligonucleotides 5′-End-Grafted onto a Gold Electrode Surface

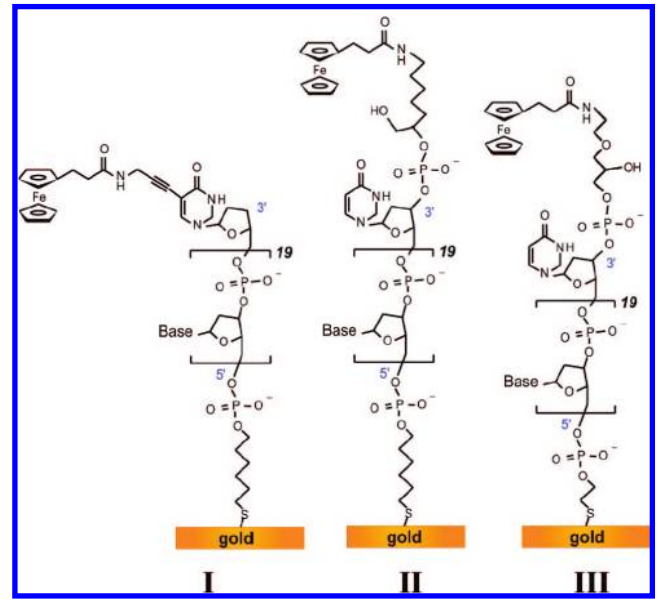

(1) (a) Boon, E. M.; Barton, J. K. *Curr. Opin. Struct. Biol.* **2002**, *12*, 320–329. (b) Giese, N. *Acc. Chem. Res.* **2000**, *33*, 253–260. (c) Schuster, G. B. *Acc. Chem. Res.* **2000**, *33*, 253–260. (d) Carell, T.; Behrens, C.; Gierlich, J. *Org. Biomol. Chem.* **2003**, *1*, 2221–2228.
(2) Kelley, S. O.; Jackson, N. M.; Hill, M. G.; Barton, J. K. *Angew. Chem., Int. Ed.* **1999**, *38*, 941–945.
(3) Anne, A.; Bouchardon, A.; Moiroux, J. *J. Am. Chem. Soc.* **2003**, *125*, 1112–1113.
(4) Anne, A.; Demaille, C. *J. Am. Chem. Soc.* **2006**, *128*, 542–557.
(5) Gorodetsky, A A.; Green, O.; Yavin, E.; Barton, J. K. *Bioconjugate Chem.* **2007**, *18*, 1434–1441.

10.1021/ja801074m CCC: $40.75

al. concluded that electronic coupling of the redox label to the base pair stack, either via intercalation or via a conjugated linker, is necessary for DNA mediated electrochemistry, a conclusion falling in line with previous results.[6] An important consequence of this restraining condition is that molecular motion of the whole dsDNA strand is left as the sole plausible charge transport mechanism for the numerous redox-dsDNA systems where such an electronic coupling is lacking.[5]

Concomitantly, Plaxco, Heeger et al. showed that the actual signaling mechanism of electrochemical DNA sensors (E-DNA sensors)[7] implies collision of the redox head with the electrode surface.[8] These sensors usually consist of a layer of redox end-labeled single-stranded (ss) probe-DNA strands, either linear or forming a stem-loop,[7,9] thiol end-grafted onto surfaces via an alkyl linker, usually a six-carbon (C_6) alkyl linker. It was consequently concluded that the sensitivity of E-DNA sensors toward detection of the complementary target probe in solution resulted from the changes of motional dynamics of the end-grafted DNA probe upon hybridization,[8] a result in agreement with our earlier work.[3]

Many other types of electrochemical DNA sensors, not necessarily involving terminal attachment of the redox label to the DNA probe, are also reported in the literature.[10] However, no matter the exact design of the sensor, the question arises: what is the nature of the electron-transport process within end-anchored DNA layers?

It is therefore highly desirable to gain more insights, preferably *quantitative* insights, into the way molecular motion of end-anchored redox-DNA strands actually contributes to the electrochemical response of redox-DNA layers. Studying the dependence of the electrochemical behavior of these layers as a function of the chemical structure of the end-grafted DNA strands can yield useful information for the optimization of the performances of E-sensors. Equivalently, but more fundamentally, considering the experimental difficulty in addressing the properties of nanometer-sized DNA strands (oligonucleotides),[11] it is also of a great interest to determine which information can be gained regarding the physical properties of short DNA strands from the electrochemical study of end-anchored redox-DNA systems.

In this context, the first aim of the present work is to investigate the respective roles of the surface-linker, connecting the DNA probe to the electrode surface, and of the Fc-linker, connecting the Fc head to the probe DNA strand, on the electrochemical response of end-grafted Fc-DNA systems. To achieve this goal two low-density Fc-DNA systems, denoted **I** and **II** in Chart 1, both anchored to a gold surface via a commonly used C_6 linker, but differing by a markedly dissimilar chemical structure of their Fc linkers, are assembled onto gold electrodes. Oligothymine (dT) sequences are chosen for all of the Fc-DNA "model" systems studied here since it is well established that thiolated-oligo(dT) chains have the property of forming well-defined end-anchored layers on bare gold surfaces.[3,12–14] The voltammetric behavior of these Fc-DNA-C_6 systems are studied and compared one with another and with the one we previously reported for the C_2-anchored Fc-DNA system **III**.

The second purpose of this work is to develop a suitable model allowing the voltammetric response of C_6-end-anchored redox-DNA systems to be quantitatively described on the basis of parameters related to the underlying dynamics of the DNA chain itself. It is hoped that this model will, in the future, allow the electrochemical behavior of redox-DNA systems to be compared one with another on the basis of physically relevant parameters.

The role of DNA-mediated charge transfer is also investigated by comparing the voltammetric behavior of a layer of end-anchored Fc-DNA probe hybridized with perfectly matched and mismatched strands.

2. Experimental Section

Materials. The precursor sequence 3′-$(dT)_{19}$-C_6-5′ oligonucleotide featuring a $(CH_2)_6$-S-S-$(CH_2)_6$-OH protected thiol at the 5′-terminus was purchased from Cybergène (Evry, France). All other ferrrocene-unlabeled DNA oligonucleotides were purchased from Eurogentec (Seraing, Belgium) and were Oligold purified grade products.

All chemicals and solvents were analytical grade and used without further purification. All reactions were carried out in polypropylene tubes under an inert atmosphere and protected from light. All aqueous solutions were made with Milli-Q purified water (Millipore). Phosphate buffer was made of 49 mM pH adjusted to 7.0 with a 1 M NaOH solution.

Cyclic Voltammetry Measurements. Aqueous 1 M $NaClO_4$ containing 25 mM phosphate buffer (pH 7.0) was used as the electrolyte solution for all electrochemical studies. Electrochemical experiments were performed with a conventional three-electrode configuration consisting of a gold-disk working electrode, a platinum wire counter electrode, and a KCl saturated calomel electrode (*SCE*) reference electrode. The *SCE* reference electrode was separated from the supporting electrolyte solution with a bridge terminated with a glass frit, containing, for the characterization of the Fc-DNA layers, an aqueous solution of 1 M NaCl. For the electrochemical pretreatment of the gold electrodes the bridge contained 1 N H_2SO_4. The peak potentials were measured with an accuracy of ±5 mV. For potential scan rates υ up to 500 V/s, all electrochemical experiments were performed using a conventional instrumentation equipment.[15a] For high scan rate cyclic voltammetry of the DNA-modified electrodes, the signal generator was a Hewlett-Packard 3314A, and the curves were recorded with a Tektronix TDS 430A oscilloscope with a minimum acquisition time of 5 ns

(6) Inouye, M.; Ikeda, R.; Takase, M.; Tsuri, T.; Chiba, J. *Proc. Natl. Acad. Sci. U.S.A.* **2005**, *102*, 11606–11610.
(7) (a) Fan, C.; Plaxco, K. W.; Heeger, A. J. *Proc. Natl. Acad. Sci. U.S.A.* **2003**, *100*, 9134–9137. (b) Immoos, C. E.; Lee, S. J.; Grinstaff, M. W. *ChemBioChem* **2004**, *5*, 1100–1104.
(8) Ricci, F.; Lai, R. Y.; Heeger, A. J.; Plaxco, K. W.; Sumner, J. J. *Langmuir* **2007**, *23*, 6827–6834.
(9) Ricci, F.; Lai, R. Y.; Plaxco, K. W *Chem. Commun.* **2007**, 3768–3770.
(10) (a) Odenthal, K. J.; Gooding, J. J. *Analyst* **2007**, *132*, 603–610. (b) Gooding, J. J. *Electroanalysis* **2002**, *14*, 1149–1157, and references therein.
(11) (a) Lankaš, F. *Biopolymers* **2004**, *73*, 327–339, and references therein. (b) Wiggins, P. A.; Van der Heijden, T.; Moreno-Herrero, F.; Spakowitz, A.; Phillips, R.; Widom, J.; Dekker, C.; Nelson, P. C. *Nat. Nanotechnol.* **2006**, *1*, 137–141.
(12) (a) Kimura-Suda, H.; Petrovykh, D. Y.; Tarlov, M. J.; Whitman, L. J. *J. Am. Chem. Soc.* **2003**, *125*, 9014–9015. (b) Petrovykh, D. Y.; Pérez-Dieste, V.; Opdahl, A.; Kimura-Suda, H.; Sullivan, J. M.; Tarlov, M. J.; Himpsel, F. J.; Whitman, L. J. *Langmuir* **2004**, *20*, 429–440. (c) Kimura-Suda, H.; Petrovykh, D. Y.; Tarlov, M. J.; Whitman, L. J. *J. Am. Chem. Soc.* **2006**, *128*, 2–3.
(13) (a) Storhoff, J. J; Elghanian, R; Mrkin, C. A; Letsinger, R. L. *Langmuir* **2002**, *18*, 6666–6670. (b) Demers, L. M.; Östblom, M.; Zhang, H.; Jang, N.-H.; Liedberg, B.; Mirkin, C. A. *J. Am. Chem. Soc.* **2002**, *124*, 11248–11249.
(14) Wolf, L. K.; Gao, Y.; Georgiadis, R. M. *Langmuir* **2004**, *20*, 3357–3361.
(15) (a) Anne, A.; Demaille, C.; Moiroux, J. *J. Am. Chem. Soc.* **1999**, *121*, 10379–10388. (b) Anne, A.; Demaille, C.; Moiroux, J. *J. Am. Chem. Soc.* **2001**, *123*, 4817–4825.

per point; a home-built potentiostat with a large bandwidth was used.[16] This ultrafast equipment, associated with a low solution ohmic drop, rendered minimal by the high conductivity of aqueous 1 M $NaClO_4$ supporting electrolyte, allowed the reliable electrochemical measurement of grafted Fc-DNA electrode responses with no detectable distortion of the signals. Cyclic voltammograms were recorded without ohmic drop compensation. All potentials are reported versus *SCE*. The temperature in all electrochemical experiments was 20 °C.

Synthesis of the 5′-C_6-Protected Thiol 3′-Ferrocene-modified Oligonucleotides. The Fc-C_7-$(dT)_{20}$-C_6 oligonucleotide, featuring a protected thiol function linked to the 5′-terminus via a C_6 alkyl linker, and a ferrocene moiety linked to the 3′-terminus via a $CHCH_2OH(CH_2)_5$ (C_7) linker was prepared as its disulfide [Fc-C_7-$(dT)_{20}$-$C_6S]_2$-dimer, and purified as already described.[17] The redox labeled FcddU-$(dT)_{19}$-C_6-5′ oligonucleotide, carrying a ferrocene 2′-deoxyuridine unit linked to the 3′-terminus, was prepared by enzymatic TDT 3′-end labeling of 3′-$(dT)_{19}$-C_6-5′ oligonucleotide using a FcddUTP nucleotide terminator[18] following a procedure modified from reference 18. Approximately 5 nmol of 3′-$(dT)_{19}$-C_6-5′ (~10 μM) and 100 nmol of FcddUTP (0.21 mM) in TDT reaction buffer (480 μL) containing 25 mM Tris-HCl and 100 mM potassium cacodylate, pH 7.2, 5 mM $CoCl_2$ and 0.2 mM dithiothreitol were mixed with 500 units (20 μL) of terminal deoxynucleotidyl transferase TDT (Roche Molecular Biochemicals (Boehringer, Mannheim)). The reaction was allowed to proceed for 3 h at 37 °C. Then the mixture was passed over a C_{18} Sep-Pak cartridge (Waters Millipore Corp (Milford, MA)).TDT enzyme, reaction buffer components, and unreacted ferrocene were removed by washing gradually the cartridge with 0.1 M aqueous triethylammonium acetate pH 7.0 (eluent A) containing from 10% to 15% acetonitrile. The desired ferrocene oligonucleotide was further eluted from the column with about 3 mL of 25% acetonitrile in A. The collected fractions were concentrated by lyophilization, and then purified by HPLC on a reverse phase C18 column with acetonitrile and triethylammonium acetate as the eluents. Appropriate fractions were collected and lyophilized to afford the oligonucleotide extended at the 3′-end with a FcddU label, FcddU-$(dT)_{19}$-C_6-5′. Average isolated yield 75%. MS (MALDI-TOF) (+) data: *m/z* $(M + H)^+$, 6614.02, $C_{227}H_{299}N_{41}O_{142}P_{20}S_2Fe$ requires 6613.50.

Pretreatment of the Polycrystalline Gold Electrodes. Gold disk working electrodes were constructed by sealing lengths of gold wire (99.99%, Goodfellow) (0.5 mm diameter) within polypropylene bodies. For all experiments, the electrodes were polished to a mirror finish using progressively finer grades of alumina polishing suspensions (3, 0.5 and 0.05 μm, Buehler) followed by ultrasonication in water and ethanol. The freshly polished electrodes were electrochemically cleaned by cyclic voltammetry at the scan rate of 0.2 V s^{1-} in 1 N H_2SO_4 as reported previously.[19] The final electrochemical oxidation step was followed by electrochemical reduction of the gold oxide monolayer via a reverse potential scan down to + 0.2 V. The thus pretreated gold electrodes were quickly rinsed with water and ethanol, and then immediately used for reaction with thiolated Fc-DNA. The effective areas of the electrodes S_{eff}, were derived from the charge associated with the gold oxide reduction peak and typically correspond to a roughness factor of ~3.

Preparation of Fc-DNA-C_6-Modified Gold Electrodes. The thiolated oligonucleotides Fc-DNA-C_6SH were prepared immediately before use by reduction of the corresponding disulfide, and HPLC purified, as described previously.[17] The final aqueous assembly solution contained ~30 μM of 5′-thiol-terminated oligonucleotide in triethylammonium acetate, Et_3NH^+, AcO^- (TEAA, ~0.35 M), pH 7.0. Self-assembly of the Fc-DNA layer was carried out as described in the Results section.

TDT-Mediated 3′ FcddU Redox End Labeling of a $(dT)_{19}$-C_6-Modified Gold Electrode. Enzymatic FcddU redox labeling was performed as previously described,[20] by incubating $(dT)_{19}$-reactant gold surface with TdT recombinant (Roche Diagnostics, France), in a Tris-HCl buffer solution containing ~60 μM of a FcddUTP nucleotide terminator at 37 °C for 2 min. We previously demonstrated that following such a procedure TdT incorporates rapidly and quantitatively the Fc-labeled chain terminator at the free 3′-end of the $(dT)_{19}$ monolayer to yield a molecular layer of FcddU-$(dT)_{19}$-C_6 whose structure is detailed in Chart 1.

Hybridization of the Fc-ssDNA Surfaces. See Results and Discussion sections.

Dehybridization of the Fc-dsDNA Surfaces. Dehybridization of the end-grafted Fc-$(dT\text{-}dA)_{20}$ and Fc[ddU-$(dT)_{19}(dA)_{20}$]-strands was carried out by soaking the gold electrodes in a 10 mM $NaClO_4$ solution at room temperature for ~12 h. As previously reported, this gentle dehybridization technique yields slow but complete dehybridization of the end-grafted Fc-dsDNA at room temperature. Comparison of the low scan rate cyclic voltammograms recorded before and after dehybridization showed that no chain loss occurred during dehybridization.

3. Results

3.1. Characterization of the FcddU-$(dT)_{19}$-C_6 Modified Gold Electrode, Fc-DNA-C_6 SystemI. 3.1.1. Assembly and Characterization of the Single-Stranded Layer by Cyclic Voltammetry. A molecular monolayer of FcddU-$(dT)_{19}$-C_6 strands was 5′-thiol end-grafted onto a polycrystalline gold electrode surface by reacting the electrode with a ~10 μM solution of FcddU-$(dT)_{19}$-C_6-SH for ~16 h under argon (see Experimental Section).

The resulting FcddU-$(dT)_{19}$-C_6-modified gold electrode was immersed in a 1 M $NaClO_4$ aqueous solution and characterized by cyclic voltammetry. As exemplified in Figure 1a (blue trace), for scan rates up to υ = 100 V/s the cyclic voltammogram of the FcddU-$(dT)_{19}$-C_6 electrode displays a remarkable reversible faradaic signal, whose features are as expected for an ideal Nernstian surface-bound species such as Fc-ssDNA:[3,4] the peak heights are proportional to the scan rate υ, and the peak-to-

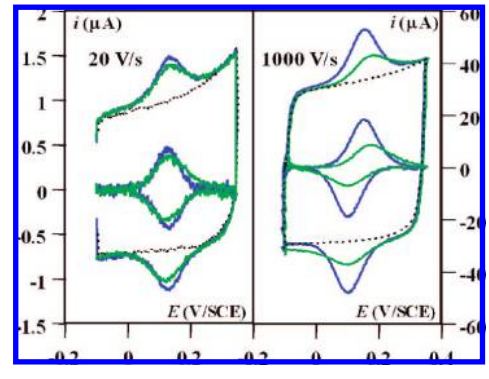

Figure 1. Cyclic voltammograms at a 0.5 mm diameter gold disk electrode bearing a 5′-end-grafted low density layer of FcddU-$(dT)_{19}$-C_6, **I**, before hybridization (blue trace) and after complete hybridization of the layer by complementary unlabeled dA_{20} strands (green trace). The scan rate is: (a) υ = 20 V/s and (b) υ = 1000 V/s. The dashed curves correspond to background signals recorded after the DNA layer was cathodically stripped. Raw and background subtracted signals are shown. Temperature T = 20 °C. Supporting electrolyte: 1 M $NaClO_4$ + 25 mM sodium phosphate buffer pH 7. Surface coverage $\Gamma = 4 \times 10^{-12}$ mol/cm^2.

(16) Hapiot, P.; Moiroux, J.; Savéant, J.-M. *J. Am. Chem. Soc.* **1990**, *110*, 1337–1343.
(17) Wang, K.; Goyer, C.; Anne, A.; Demaille, C. *J. Phys. Chem. B* **2007**, *111*, 6051–6058.
(18) Anne, A; Blanc, B.; Moiroux, J. *Bioconjugate Chem.* **2001**, *12*, 396–405.
(19) Anne, A.; Demaille, C.; Moiroux, J. *Macromolecules* **2002**, *35*, 5578–5586.

peak separation is less than 10 mV, indicating that charge transfer kinetics does not interfere.

The standard potential of the Fc head, as determined from the common value of the anodic and cathodic peak potentials, $E° = 130 \pm 10$ mV/SCE, is close to the one previously reported for Fc-ssDNA freely diffusing in aqueous solutions,[3,4] showing that the environment experienced by the Fc heads borne by the strands is similar in both cases. In addition, the peak width at midpeak height is ~95 mV, which is close to the predicted value of 90 mV for identical, non-interacting tethered redox centers, located outside the double layer.[21] Therefore, integration of the background-subtracted peak currents provided the coverage in Fc heads, and hence in FcddU-$(dT)_{19}$-C_6 chains. The chain coverage thus found was $(2-4) \times 10^{-12}$ mol/cm^2 (per effective electrode surface area); this value corresponds to an average interchain distance of ~7−9 nm, which is comparable to the overall length of the FcddU-$(dT)_{19}$-C_6 molecule $L_{ss} \approx 12$ nm [contour length of ddU-$(dT)_{19}$ = 10 nm,[22] + ~1.8 nm,[23] for the surface C_6 and Fc linkers (see Chart 1)]. As a result, lateral interactions between neighboring grafted chains are minimal for this system.[24]

At high scan rates (υ > 100 V/s), and as shown in Figure 1b, the voltammograms retained their symmetrical morphology typical of surface signals. However, the peak-to-peak separation increases due to the contribution of the rate of the heterogeneous electron transfer to the kinetic control of the faradaic current.

As seen in Figure 2a (open symbols), the ratio of the anodic peak current, i_{pa}, over the scan rate remained approximately constant up to $\upsilon \approx 1000$ V/s, indicating that motional dynamics of the ferrocene head of FcddU-$(dT)_{19}$-C_6 (i.e., the frequency at which the Fc head collides with the electrode) is too fast to be accessed within the scan rate range we explored.

The scenario of a flat-lying (adsorbed) FcddU-$(dT)_{19}$-C_6 strand, which would result in identical voltammetric characteristics, is made unlikely by the fact that oligo(dT) sequences were repeatedly shown to display low adsorption affinity for bare gold surfaces.[3,12–14] Accordingly, cyclic voltammetry studies of Fc-$(dT)_{20}$ in solution, that we reported previously, did not show any sign of adsorption of the Fc-DNA chains.[4] Moreover AFM-SECM studies of the very same DNA system considered here showed that the Fc head of FcddU-$(dT)_{19}$-C_6 explores a volume above the surface compatible with free thermal motion of the end-grafted strand in a fully elongated conformation.[20] Under such conditions the voltammetric behavior of the system is identical to the one of a thin layer cell (TLC),[25] of a thickness comparable with the overall length of the strand, within which the Fc head diffuses rapidly. This behavior can be quantitatively described as reported by Laviron for the case of a slow electron transfer to a surface-confined species.[26] The variation of E_{pa} and E_{pc} can then be fitted using an overall apparent electron transfer rate k_0 as a single

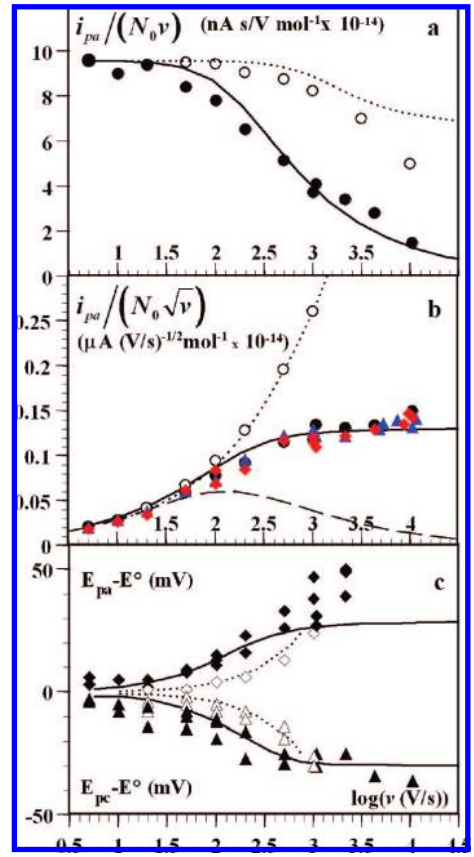

Figure 2. Scan rate, υ, dependence of the anodic peak current i_{pa} and of the anodic and cathodic peak potentials, E_{pa} and E_{pc}, of the cyclic voltammograms recorded at a gold electrode bearing a 5′-end-grafted layer of FcddU-$(dT)_{19}$-C_6, **I**, before (open symbols) and after (filled symbols) hybridization by: fully complementary $(dA)_{20}$ (black symbols), mismatching 5′-$(dA)_{10}$dC$(dA)_9$-3′ (blue triangles), and mismatching 5′-$(dA)_{10}$dG$(dA)_9$-3′ (red diamonds). In (a) and (b) the peak current is normalized versus υ and $(\upsilon)^{1/2}$ respectively, and versus the total amount of Fc heads ($N_0 = S_{eff} \times \Gamma$). The continuous lines correspond to a theoretical fit of the data obtained for the hybridized DNA layer, using the rotational diffusion model with $D_r = 2300$ s^{-1}, $\Lambda = \infty$. The dotted line corresponds to a fit of the data obtained for the nonhybridized DNA layer, using Laviron's theory for surface-bond species (TLC model) with a transfer coefficient $\alpha = 0.5$ and $k_0 = 2 \times 10^4$ s^{-1}.[23] The dashed line in (b) represents the theoretical $i_{pa}/(\upsilon)^{1/2}$ vs $\log(\upsilon)$ variation calculated using the elastic bending model previously reported, which describes the motion of the Fc head as resulting from elastic bending of the duplex, and reproduces the experimental behavior of a layer of Fc-$(dT)_{20}$-C_2, **III**, hybridized by $(dA)_{20}$.

experimental parameter. As seen in Figure 2c this yields a reasonable agreement between the experimental (white diamonds) and calculated (dotted curve) peak potential variations, and to a best fit value of $k_0 = (2 \pm 0.5)\ 10^4$ s^{-1}. For the TLC model k_0 is related to ε, the apparent thickness of the layer, and k_s, the heterogeneous rate constant for the electron transfer between the electrode and the Fc head: $k_0 = k_s/\varepsilon$. Taking $\varepsilon = L_{ss} = 12$ nm one obtains: $k_s \approx (2.4 \pm 0.6) \times 10^{-2}$ cm/s. This k_s value is comparable to the one measured for freely diffusing Fc-tagged ssDNA chains **III** in solution, which was of $(5 \pm 2) \times 10^{-2}$ cm/s.[4]

For υ > 1000 V/s we consistently observed that the i_{pa}/υ ratio decreased below the value predicted by the TLC model (see dotted line in Figure 2a). This indicates that, for $\upsilon \approx 1000$V/s, the observation time of cyclic voltammetry, $t_{cv} = RT/F\upsilon$, becomes sufficiently short to be in the order of t_{ss}, the motional time characterizing the dynamics of FcddU-ssDNA. Therefore,

(20) Anne, A.; Bonnaudat, C.; Demaille, C.; Wang, K. *J. Am. Chem. Soc.* **2007**, *129*, 2734–2735.
(21) Smith, C. P.; White, H. S. *Anal. Chem.* **1992**, *64*, 2398–2405.
(22) Mills, J. B.; Vacano, E.; Hagerman, P. J. *J. Mol. Biol.* **1999**, *285*, 245–257.
(23) As measured from molecular models.
(24) Rant, U.; Arinaga, K.; Fujita, S.; Yokoyama, N.; Abstreiter, G.; Tornow, M. *Langmuir* **2004**, *20*, 10086–10092.
(25) Hubbard, A. T.; Anson, F. C. In *Electroanalytical Chemistry*; Bard, A. J., Ed.; Marcel Dekker: New York, 1982; Vol. 4, pp 129−214..
(26) (a) Laviron, E. Voltammetric Methods for the Study of Adsorbed Species. In *Electroanalytical Chemistry*; Bard, A. J., Ed.; Marcel Dekker: New York, 1982; Vol. 12, pp 53−157. (b) Laviron, E. *J. Electroanal. Chem.* **1979**, *101*, 19–28.

one can estimate that $t_{cv} > t_{ss}$, i.e. that t_{ss} is less than 0.1 ms ($1/t_{ss} > 10^4$ s^{-1}).

3.1.2. Cyclic Voltammetry Behavior of the Posthybridized Layer.

3.1.2.1. Perfectly Matched Duplex: Hybridization by the Fully Complementary $(dA)_{20}$ Target. The FcddU-$(dT)_{19}$-C_6-bearing electrode was immersed in a ~10 μM solution of fully complementary $(dA)_{20}$ target in 1 M $NaClO_4$ (50 mM sodium phosphate buffer, pH 7.0) solution at 20 °C for ~2 h to yield the fully hybridized layer.

As seen in Figure 1a (green trace), at slow scan rates ($v <$ 100 V/s), the voltammogram recorded for the hybridzed layer is very similar to the one recorded before hybridization and also displays all the characteristics of a Nernstian surface signal. Such a behavior ascertains that all the Fc heads are given sufficient time to reach the electrode surface. The measured $E°$ for the Fc head borne by the DNA duplex is ~130 ± 10 mV/SCE. This value is similar to the one measured for single-stranded FcddU-$(dT)_{19}$-C_6 showing that the environment experienced by the Fc head is unaltered by hybridization. Integration of the voltammogram yields a surface coverage which is ~15% less than the value obtained before hybridization, showing that chain loss upon hybridization is minimal. Considering that the contour length of $(dT)_{20}(dA)_{20}$ is ~6.8 nm[22] and taking ~2 nm for the length of the linkers,[23] the overall length L_{ds} of Fc[ddU-$(dT)_{19}(dA)_{20}$]-C_6 is estimated to be ~9 nm, i.e. ~3 nm shorter than FcddU-$(dT)_{19}$-C_6. As a result lateral interactions between the anchored DNA chains within the hybridized layer are expected to be even weaker than before hybridization.

As the scan rate is raised above 100 V/s, the voltammetric behavior of the hybridized layer departs significantly from the ideal surface behavior recorded before hybridization. As seen in Figure 2a (filled symbols), the i_{pa}/v ratio decreases sharply down to very low values reached for $v \geq$ 1000 V/s. In this regime the dsDNA signal is notably less intense than the one recorded before hybridization (compare blue and green traces in Figure 1b), indicating slower dynamics for FcddU-dsDNA as compared to that for FcddU-ssDNA. However, even at such high scan rates the hybridized layer gives rise to a faradaic signal that is easily distinguished from the background current (Figure 1b). Indeed, subtracting the background current, recorded at the electrode after the DNA layer has been cathodically stripped (black dotted traces in Figure 1), from the overall signal allows the faradaic component of the voltammogram to be extracted straightforwardly and accurately up to the highest scan rates explored, where the capacitive current tends to dominate the signal. As a result, and as seen in Figure 3a−d, well-defined background-corrected voltammograms can be obtained for scan rates up to $v = 5000$ V/s and faster. Strikingly, when the faradaic signal is plotted as $i/(v)^{1/2}$ versus potential (Figure 3), the signal magnitude remains almost constant over a scan rate range covering 1 order of magnitude, from 500 V/s up to 5000 V/s. Moreover, the morphology of the voltammograms is then typical of a species undergoing free diffusion.

This peculiar behavior can be conveniently visualized by plotting the peak current function, defined as the $i_{pa}/(v)^{1/2}$ ratio, vs log(v), as presented in Figure 2b (filled symbols). It is seen that, whereas the peak current function recorded for the FcddU-ssDNA layer increases continuously with scan rate, as expected for a surface process (open symbols), the variation of the peak current function for the duplex deviates from this surface-like regime to become clearly plateau-shaped from $v >$ 500 V/s. For $v >$ 2000 V/s, and as the scan rate is raised, the peak current

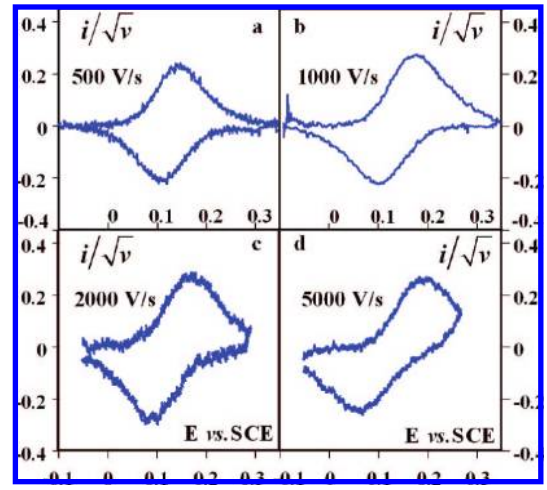

Figure 3. Cyclic voltammograms at a 0.5 mm diameter gold disk electrode bearing a 5′-end-grafted layer of FcddU-$(dT)_{19}$-C_6, **I**, layer hybridized by fully complementary $(dA)_{20}$ target strands. The scan rate v is indicated near each voltammogram. The current (i in μA) is normalized by $(v)^{1/2}$. The signals recorded after cathodic stripping of the DNA layer were used as backgrounds and subtracted from the raw signals. Background-subtracted signals are shown. Temperature $T = 20$ °C. Supporting electrolyte: 1 M $NaClO_4$ + 25 mM sodium phosphate. buffer pH 7. Fc-DNA surface coverage $\Gamma = 4 \times 10^{-12}$ mol/cm^2.

function is seen to depart from the plateau and to increase very slightly. This minute deviation from the plateau may be equivalently attributed to *a very small amount* of *either* unhybridized chains *or* adsorbed Fc-DNA chains, both giving rise to surface signals characterized by continuously increasing $i_{pa}/(v)^{1/2}$ vs log(v) variations.

The variations of E_{pa} and E_{pc}, the anodic and cathodic peak potentials of the voltammograms, are plotted in Figure 2c. It is seen that for $v >$ 50 V/s and up to 200 V/s the anodic peak shifts positively and the cathodic peak shifts negatively. For v = 200−1000 V/s, E_{pa} and E_{pc} remain approximately constant, and the peak-to-peak separation $\Delta E_p = E_{pc} - E_{pa}$ is then in the 60−80 mV range.

Importantly, we observed that following dehybridization of the end-grafted Fc-dsDNA strands, carried out under mild conditions (see Experimental Methods), the voltametric behavior of the Fc-ssDNA layers was fully restored. This result provides evidence that, as previously shown for the C2-anchored DNA system (**III**),[3] the electrochemical behavior of the Fc-DNA-C6 layer is specifically (and reversibly) modulated by the hybridization/dehybridation of the anchored Fc-DNA chains. Finally, it is noteworthy that a voltammetric behavior identical to the one described above was also observed for C_6-dT_{19} 5′-thiol end-grafted onto gold electrodes, and subsequently surface 3′-end-labeled by TDT enzyme in the presence of the FcddU nucleotide terminator. This result confirms that surface labeling of end-anchored C_6-dT_{19} chains by TDT/FcddU is a convenient way to produce well-defined FcddU-$(dT)_{19}$-C_6 layers.[20]

3.1.2.2. Behavior of the Single-Base Mismatched Duplexes. In separate experiments FcddU-$(dT)_{19}$-C_6 bearing electrodes were hybridized by 5′-$(dA)_{10}dC(dA)_9$-3′ and 5′-$(dA)_{10}dG(dA)_9$-3′ targets to yield respectively CT and GT mismatched duplexes. The targets were selected so that the single-base mismatch would be positioned close to the center of the duplex. This is expected to lower the melting temperature of the hybridized strand in solution from ~55 °C for the perfectly matched case down to

~46 °C for both the CT and GT mismatched case (1 M Na^+),[27] this value is *a priori* still sufficiently higher than the working temperature of 20 °C to ensure stability of the duplex during the voltammetric characterization. This predicted stability is confirmed by the observed perfect repeatability of the signals recorded over several hours.

Both of the mismatched duplexes examined here were observed to give rise to a voltammetric behavior identical to the one described above for the perfectly matched duplex. This is exemplified in Figure 2b where the variation of the peak current function vs log(v) for the mismatched and perfectly matched duplexes are compared. One can see that the variations corresponding to the CT mismatch (blue triangle), GT mismatch (red diamond), perfect match (black circle) are indistinguishable. This result excludes electron conduction through the dsDNA base stack (so-called DNA CT)[2] as a possible charge transport mechanism for the present system, since DNA CT is extremely dependent on the presence of mismatched bases in the DNA base stack.[28]

The above voltammetric behavior for the hybridized FcddU-$(dT)_{20}$-C_6 layer differs significantly from the one we previously reported for an experimental system consisting of a hybridized layer of Fc-$(dT)_{20}$-C_2 **III**, (see Chart 1), for which a characteristic bell-shaped (and not a plateau-shaped) variation of the peak current function vs log(v) was observed.[4] As can be seen from Chart 1, these experimental systems differ by a markedly dissimilar chemical structure and/or length of: (i) the linker between the Fc head and the DNA chain (Fc linker) and (ii) the linker between the DNA and the electrode (surface linker). In order to assess independently the role of these linkers on the voltammetric behavior of the redox-DNA layers, a layer of Fc-C_7-$(dT)_{20}$-C_6,**II**, which bares a Fc linker similar to **I** and a thiol linker similar to **III** was assembled onto a gold electrode and its voltammetric behavior characterized.

3.2. Characterization of the Fc-C_7-$(dT)_{20}$-C_6-Modified Gold Electrode, Fc-DNA-C_6 System II.

3.2.1. Assembly and Characterization of the Single-Stranded Layer by Cyclic Voltammetry. Assembly of the Fc-C_7-$(dT)_{20}$-C_6 layer on a gold electrode surface was carried out by reacting the freshly HPLC-purified 5′-thiol-terminated Fc-C_7-$(dT)_{20}$-C_6-SH oligonucleotide with the gold electrode for about 16 h at ambient temperature in a deaerated solution protected from light (see Experimental Section). The modified gold surface was then carefully washed with 1 M aqueous $NaClO_4$ and characterized by cyclic voltammetry in the same medium. As seen from Figure 4a (open symbols), the voltammetric behavior of the Fc-C_7-$(dT)_{20}$-C_6 layer is typical of the one of a surface confined species: the i_{pa}/v ratio remains almost constant up to 1000 V/s. The peak-to-peak separation remains less than 10 mV up to $v = 50$ V/s allowing a value of $E° = 140$ mV/SCE to be derived for the standard potential of the Fc head from the value of the anodic and cathodic peak potentials. Integration of the voltammograms yields a coverage in Fc heads (and thus in Fc-C_7-ssDNA) of $2-3 \times 10^{-12}$ mol/cm^2, showing that low-density layers are assembled.

As seen in Figure 4 (open symbols), for $v > 100$ V/s, the i_{pa}/v ratio (Figure 4a) is observed to decrease slightly and the peak-to-peak separation to increase (Figure 4c). AFM/SECM characterization of a layer of grafted Fc-C_7-$(dT)_{20}$-C_6 showed that the end-anchored chains were undergoing free thermal motion above the surface.[17] It is thus reasonable to conclude that the surface regime observed for Fc-C_7-ssDNA layers is due to the ssDNA chains undergoing fast motional dynamics, and to interpret the present results on the basis of the TLC model. Proceeding as described above this yields a value of: $k_0 = (1.5 \pm 0.5)\ 10^4\ s^{-1}$. Taking for the contour length of $(dT)_{20}$ of ~10 nm[22] and taking this time ~2.3 nm for the length of the linkers,[23] the overall length L_{ss} of Fc-C_7-$(dT)_{20}$-C_6 is estimated to be ~12.3 nm. Consequently, taking $\varepsilon = L_{ss}$ the TLC model yields: $k_s \approx (1.9 \pm 0.5) \times 10^{-2}$ cm/s. This k_s value is close to, albeit slightly smaller than, the one measured for a layer of Fc-C_7-ssDNA chains **I**. For $v = 1000$ V/s the i_{pa}/v ratio is observed to be slightly lower than expected from the TLC model (Figure 4a), pointing to a motional time t_{ss} of the single-stranded chains such that: $t_{ss} < 0.1$ ms.

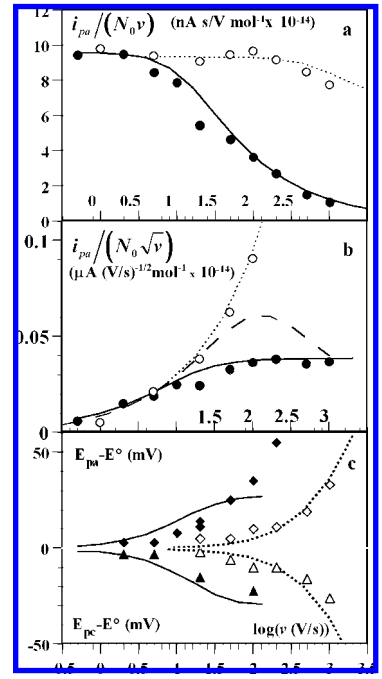

Figure 4. Scan rate, v, dependence of the anodic peak current, i_{pa}, and of the anodic and cathodic peak potentials, E_{pa} and E_{pc}, of the cyclic voltammograms recorded at a gold electrode bearing a 5′-end-grafted layer of Fc-C_7-$(dT)_{20}$-C_6, **II**, before (open symbols) and after (filled symbols) hybridization by the fully complementary $(dA)_{20}$. In (a) and (b) the peak current is normalized versus v and $(v)^{1/2}$, respectively, and versus the total amount of Fc heads ($N_0 = S_{eff} \times \Gamma$). The continuous lines correspond to a theoretical fit of the data obtained for the hybridized DNA layer, using the rotational diffusion model with $D_r = 200\ s^{-1}$, $\Lambda = \infty$. The dotted line corresponds to a fit of the data obtained for the nonhybridized DNA layer, using Laviron's theory for surface-bound species (TLC model) with a transfer coefficient $\alpha = 0.5$ and $k_0 = 1.5 \times 10^4\ s^{-1}$.[23] The dashed line in (b) represents the theoretical $i_{pa}/(v)^{1/2}$ vs log(v) variation calculated using the elastic bending model previously reported, which describes the motion of the Fc head as resulting from elastic bending of the duplex, and reproduces the experimental behavior of a layer of Fc-$(dT)_{20}$-C_2, **III**, hybridized by $(dA)_{20}$.

3.2.2. Cyclic Voltammetry Behavior of the Posthybridized Layer. The Fc-C_7-$(dT)_{20}$-C_6 layer was quantitatively hybridized by exposing the DNA bearing surface to a ~10 μM solution of the full complementary strand $(dA)_{20}$ in 1 M $NaClO_4$, 50 mM sodium phosphate buffer pH 7.0, for 1.5 h at 18 °C. The surface was then thoroughly washed with a 1 M $NaClO_4$ solution and characterized by cyclic voltammetry.

(27) As calculated from the *HYTHER Calculator*; Peyret, N.; SantaLucia, J., Jr. Wayne State UniversityDetroit, MI, version 1.0, using a 1 mM concentration for both strands, see. (a) SantaLucia, J. *Proc. Natl. Acad. Sci. U.S.A.* **1998**, *95*, 1460–1465. (b) Peyret, N.; Seneviratne, P. A.; Allawi, H. T.; SantaLucia, J. *Biochemistry* **1999**, *38*, 3468–3477.

(28) Kelley, S. O.; Boon, E. M.; Barton, J. K.; Jackson, N. M.; Hill, M. G. *Nucleic Acids Res.* **1999**, *27*, 4830–4837.

Scheme 1. Possible Types of Electron Transport Mechanisms: (a) Direct Electron Transfer through the DNA Base Stack (DNA CT); (b) Elastic Bending of the Fc-dsDNA rod; (c) Free Rotational Motion of the Fc-dsDNA Rod

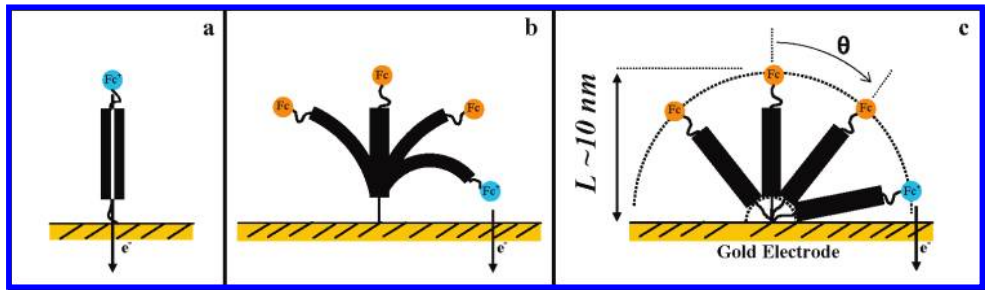

At low scan rates ($v \leq 10$ V/s) the characteristics of the recorded signals were in agreement with the ones expected for a surface confined species: the peak current was proportional to scan rate (i.e., the i_{pa}/v ratio was constant, see Figure 4a, filled symbols) and the peak separation was small ~10−20 mV (Figure 4c). The standard potential of the Fc head, derived from the common value of the anodic and cathodic peak potentials, was 140 ± 10 mV/SCE, showing that the environment experienced by the Fc head is not significantly modified upon hybridization. The surface coverage, obtained by integration of the voltammograms, was only ~20% lower than before hybridization, showing that a small number of chains was lost upon hybridization.

At higher scan rate ($v \geq 20$ V/s) the variation of the peak current function is seen to depart from the one observed before hybridization and to reach a plateau for $v > 100$ V/s (Figure 4b, filled symbols). Within the same range of scan rates the peak-to-peak separation increases to reach a value of ~70 mV at $v = 100$ V/s. Beyond 100 V/s the peak-to-peak separation increases continuously.

The prominent feature of the experimental results presented above is that, for both of the hybridized Fc-DNA-C_6 systems explored here, a clear departure from the surface regime is observed at high enough scan rate. Diffusionless electron transfer to the Fc head (DNA CT, Scheme 1a) can therefore be excluded as the electron transport mechanism within the Fc-dsDNA layers since this would have precisely resulted in the persistence of a surface behavior (i.e., scan rate-independent i_{pa}/v ratio or equivalently continuously increasing $i_{pa}/(v)^{1/2}$ ratio).[26]

Interestingly, electron transport by elastic diffusion of the Fc head, resulting from the bending of the DNA duplex toward the electrode surface (Scheme 1b), can also be excluded since, as we previously demonstrated, such a motion would have resulted in a bell-shaped $i_{pa}/(v)^{1/2}$ variation, and in an "extinction" of the faradaic signal at high scan rates.[4] At the opposite, the very fact that a very distinctive plateau can be identified in the $i_{pa}/(v)^{1/2}$ vs $\log(v)$ plot demonstrates unambiguously that molecular motion of the Fc head to and away from the electrode surface is a purely diffusional process.[29] Considering the fact that the Fc head is covalently attached to the dsDNA duplex via a linker much shorter than the contour length of the duplex, diffusion of the Fc-head toward the electrode surface necessarily results from the global motion of the dsDNA rod. The involvement of dsDNA chain motion is confirmed by the fact that we observed a slowing of the overall dynamics in high-density DNA systems, i.e. for $\Gamma \gg 2\ 10^{-12}$ mol/cm^2, where sterical interactions between neighboring end-grafted dsDNA chains are expected to hinder chain motion (data not shown).[24,30] Bearing in mind the relative stiffness of the duplex,[31] we are thus led to conclude that rotational motion of the whole C_6-anchored duplex around its anchoring point is the diffusional mechanism allowing the Fc head to approach sufficiently from the electrode to exchange an electron with it (Scheme 1c). A model, describing the voltammetric behavior of the ferrocene head diffusing as a result of the hinge motion of the DNA duplex, is described below.

4. Theory

4.1. Rotational Dynamics of an End-Anchored dsDNA Rod. Free hinge motion of the end-anchored Fc-bearing dsDNA strand can be represented as seen in Scheme 1c. Since this motion is driven by thermal agitation, the time constant describing the motional dynamics of the rod will be related to an overall rotational diffusion coefficient, D_r, representing the frictional interaction of the rod with the solvent. It is reasonable to assume that D_r will be dominated by the interactions between the DNA duplex and the solvent, the contribution of the much smaller sized linkers to the overall friction being comparatively negligible. As a result, and as a first approximation, the linkers are assumed to play no role in the overall dynamics but simply to serve as a hinge (surface linker) and to add to the effective length L of the rotating rod expressed by $L = L_{ds} + l_{Fc\ linker} + l_{surface\ linker}$.

The motion of the Fc head can therefore be described as diffusion over the hemispherical shell of radius L shown in dotted line in Scheme 1.

4.2. Cyclic Voltametry of a Species Undergoing Free Diffusion over a Hemispherical Shell. The cyclic voltammetry behavior of a redox species undergoing free diffusion over a truncated spherical shell, to reach an underlying planar electrode surface, has been originally described by Amatore[32] and later by others,[33] albeit in experimental contexts totally remote from the present work. The governing equations are therefore briefly recalled below, using a slightly different formalism.

(29) (a) Andrieux, C. P. Savéant, J.-M. Electrochemical Reactions. In *Investigations of Rates and Mechanisms of Reactions, Techniques in Chemistry*; Bernasconi, C., Ed.; Wiley: New York, 1986; Vol. 6, 4/E, Part 2, pp 305−390. (b) Bard, A. J.; Faulkner, L. R. *Electrochemical Methods: Fundamentals and Applications*, 2nd ed.; John Wiley & Sons: New York, 2000; pp 226−231..

(30) A similar "molecular crowding effect" has been recently reported by Plaxco and Heeger in ref 8, and interpreted similarly.

(31) With the persistence length of dsDNA (~50 nm) being much larger than the contour length of $(dT)_{20}$ (~10 nm), the dsDNA chain can be seen as a relatively rigid rod.

(32) (a) Amatore, C.; Bouret, A.; Maisonhaute, E.; Goldsmith, J. I.; Abruña, H. D. *Chem. Eur. J.* **2001**, *7*, 2206–2226. (b) Amatore, C.; Bouret, A.; Maisonhaute, E.; Goldsmith, J. I.; Abruña, H. D. *ChemPhysChem* **2001**, *2*, 130–134.

(33) Thompson, M.; Compton, R. G. *ChemPhysChem* **2006**, *7*, 1964–1970.

At equilibrium, when the electrode is biaised at a potential sufficiently negative for the Fc heads not to react at the electrode, free hinge motion of the rod insures that the Fc head explores all the positions available on the hemispherical shell surface. In other words, the probability density P^* of finding the Fc head in *any* circular stripe of the shell, is the same.[34] The probability dP of finding the Fc head in a given stripe of the shell having a surface area ds, is $dP = P^* ds$. Considering that for a hemispherical shell $ds = 2\pi L^2 \sin(\theta)\, d\theta$, with θ the angle from the surface normal (see Scheme 1), and that the Fc head must be found on the shell we have:

$$2\pi L^2 \int_0^{\frac{\pi}{2}} P^* \sin(\theta)\, d\theta = 1$$

which yields $P^* = 1/(2\pi L^2)$. Upon scanning the potential positively, the Fc head, when reaching the electrode surface, is oxidized as:

$$Fc \underset{k_s}{\overset{E^\circ}{\rightleftharpoons}} Fc^+ + e^-$$

where Fc and Fc^+ respectively stand for the reduced and oxidized form of the ferrocene head, E° is the standard potential of the redox couple, and k_s the rate constant for the heterogeneous electron transfer at the electrode. The Fc heads existing solely under the Fc or Fc^+ forms, their respective probability density $P(t,\theta)$ and $Q(t,\theta)$ are related by: $P(t,\theta) + Q(t,\theta) = P^*$, meaning that the rotational diffusion problem has to be solved for the reduced Fc head only.

The linear variation of the electrode potential E with time is expressed by $E = E_i + \upsilon t$, with E_i the starting potential of the scan, set at a negative enough value for the voltammogram not to depend on it, and υ the scan rate. Introducing the dimensionless potential ξ, defined as: $\xi = F(E - E^\circ)/RT$, with F the Faraday constant, the above equation becomes: $\xi = \beta\, \tau + \xi_i$.

The β parameter thus introduced, and defined as $\beta = (F\upsilon)/(RTD_r)$, compares the characteristic rotational time, D_r, to the cyclic voltammetry observation time $RT/F\upsilon$.

The probability flux j of Fc heads going toward the electrode is given by $j = -D_r \sin\theta(\partial p/\partial\theta)$. The electrode bearing N_0 mole of identically behaving dsDNA chains, the overall faradaic current i is given by $i = FN_0 j = -FN_0 D_r \sin\theta(\partial p/\partial\theta)$, N_0 is related to the coverage in dsDNA chains by: $N_0 = \Gamma S_{eff}$ with S_{eff} the effective electrode surface area. It is convenient to introduce the dimensionless current ψ, which is defined as $\psi = i/(FN_0D_r)$, and also the current function $\psi^* = \psi/(\beta)^{1/2}$, which is the dimensionless equivalent of the $i/(\upsilon)^{1/2}$ ratio used above to present the experimental data.

The time and space (angular) evolution of P, during the time course of the voltammogram, is described by the second Ficks' law, expressed in spherical coordinates and for the particular case of rotational diffusion:

$$\frac{\partial p}{\partial \tau} = \frac{\partial^2 p}{\partial \theta^2} + \frac{1}{\tan\theta}\frac{\partial p}{\partial \theta} \qquad (1)$$

with τ and p the dimensionless variables defined as $\tau = D_r\, t$, $p(\tau,\theta) = P(t,\theta)/P^*$ to which are associated the initial condition: $\tau = 0, \forall\theta: p = 1$ and the following boundary conditions.

(34) Diffusion of the single Fc head borne by the rod is described here using the notion of probability density. Diffusion of electrons between many redox sites dispersed over a single shell was equivalently described in terms of surface concentration in redox sites (ref 32).

The boundary condition at the top of the shell is: $\theta = 0: (\partial p/\partial\theta)_0 = 0$ (for reasons of symmetry).

The boundary condition at the electrode surface depends on the rate of electron transfer:

- If the electron transfer is fast enough to remain at equilibrium, then the Nernst equation applies; thus, $p(\tau,0) = 1/(1+e^{-\xi})$.
- If the electron transfer displays finite kinetics, then using the classical Butler−Volmer formalism we have the following relation: $\psi = \Lambda e^{\alpha\xi}[p(\tau,0)(1+e^{-\xi}) - e^{-\xi}]$, with α the transfer coefficient which for an outer-sphere redox species like ferrocene, can be taken as $\alpha = 0.5$. The newly introduced parameter $\Lambda = k_s/(D_rL)$ compares k_s, the rate constant for the electron transfer of the Fc head to the electrode, with the rotational rate of the rod.

The dimensionless voltammogram $\psi(\xi)$ solely depends on the β and Λ parameters and can be calculated by solving numerically eq 1.

The following experimentally relevant limiting situations can be identified:

***β* → 0, (i.e., *υ* → 0): Surface Regime.** This situation corresponds to the scan rate being slow enough as compared to the dsDNA dynamics, for the Fc heads to have ample time to exchange an electron reversibly with the electrode. In practice this situation is reachable by lowering the scan rate sufficiently. Understandably, no information regarding dsDNA dynamics can then be obtained from the signal.

The dimensionless current is then given by:

$$\psi = \beta\, \frac{\exp[-\xi]}{(1+\exp[-\xi])^2}$$

while the corresponding forward (here anodic) current is:

$$i_a = \frac{F^2 N_0 \upsilon}{RT} \frac{\exp\left[-F\frac{(E-E^\circ)}{RT}\right]}{\left(1+\exp\left[-F\frac{(E-E^\circ)}{RT}\right]\right)^2}$$

the anodic peak current is thus given by

$$i_{pa} = 0.25\frac{F^2 N_0 \upsilon}{RT}$$

This expression is identical to the one predicted for the Nernstian behavior of a redox species irreversibly adsorbed to an electrode. The anodic and cathodic peak potentials are equal to E° and the peak current is proportional to the scan rate. Integration of this surface signal leads to N_0 the total amount of Fc heads (and thus of dsDNA) present at the electrode surface.

As seen from the above equation relating i_{pa} to υ, attainment of the surface regime can be experimentally ascertained by the observation of a scan rate independent i_{pa}/υ ratio, or equivalently by the $i_{pa}/(\upsilon)^{1/2}$ ratio increasing as $(\upsilon)^{1/2}$.

***β* → +∞, (i.e., *υ* → +∞): Rotational Diffusion Regime.** This case corresponds to the scan rate being large enough for the motional time of the Fc heads to become accessible. Such a diffusional regime can, in principle, always be experimentally reached by increasing sufficiently the scan rate. The voltammogram is then identical to the one obtained in the case of a redox species undergoing semi-infinite planar diffusion.[29]

The anodic peak current is then given by

$$i_{pa} = FN_0\sqrt{D_r}\sqrt{\frac{F\upsilon}{RT}} \times \psi^*_{pa,dif} \qquad (2)$$

where $\psi^*_{pa,dif}$ is a constant which depends only slightly on the rate of electron transport at the electrode, i.e. on Λ: $\psi^*_{pa,dif} = 0.446$ for a rapid (Nernstian) electron transfer (i.e., $\Lambda \rightarrow +\infty$), $\psi^*_{pa,dif} = 0.351$ for a slow (irreversible) electron transfer (i.e., $\Lambda \rightarrow 0$).

The forward (anodic) and backward (cathodic) peak currents are symmetrically located on the potential axis, respectively at positive and at negative potentials with respect to the standard potential $E°$, so that $E° = (E_{pa}+E_{pc})/2$. For a rapid (Nernstian) electron transfer (i.e., $\Lambda \rightarrow +\infty$), the peak-to-peak separation ΔE is of ~60 mV, whereas an irreversible electron transfer is characterized by $\Delta E \gtrsim 200$ mV.

Most importantly, it can be seen from eq 2, that the diffusional regime is characterized by a scan rate independent $i_{pa}/(\upsilon)^{1/2}$ ratio. Experimental attainment of this situation can thus be ascertained by the observation of a plateau in the $i_{pa}/(\upsilon)^{1/2}$ vs $\log(\upsilon)$ plots. Once this situation is met, the value of D_r, the key parameter quantifying the rod dynamics, can be straightforwardly derived from the height of the plateau using the expression for i_{pa} given in eq 2. Interestingly the dependence of the thus derived D_r value on the rate of the heterogeneous electron transfer (i.e., on Λ) is weak: since $\psi^*_{p,dif}$ can only vary in the 0.351−0.446 interval (see above), the D_r value can be estimated within a factor 1.6 even if no information is available about the rate of heterogeneous electron transfer. However, by measuring the peak-to-peak separation, ΔE_p, the Nernstian ($\Delta E_p \approx 60$ mV) or irreversible ($\Delta E_p > \sim 200$ mV) electron transfer situation can be identified and consequently the relevant value of $\psi^*_{p,dif}$ can then be used in eq 2, allowing a more accurate value of D_r to be determined.

In the general case accurate determination of D_r requires the voltammogram to be calculated by solving numerically eq 1. The variations with β of the anodic peak current function ψ^*_{pa}, and of the peak potentials of the voltammograms $\xi_{pa,c}$, calculated for various values of Λ, are represented respectively in Figure 5a and Figure 5b. These graphs are the dimensionless equivalents of the experimental $i_{pa}/(\upsilon)^{1/2}$ and $E_{pa,c}$ vs $\log(\upsilon)$ plots.

Upon increasing β (i.e., the scan rate), from low values corresponding to the surface regime, the peak current function is seen to increase continuously until a plateau is reached, corresponding to the attainment of the rotational diffusion regime. As seen in Figure 5a, the ψ^*_{pa} vs $\log(\beta)$ variation displays little dependence on the rate of electron transfer (Λ). At the opposite finite electron transfer kinetics translates much more clearly on the variation of the peak potentials with increasing scan rate (Figure 5b). At low enough β value (i.e., scan rate) the peak potentials are equal to $E°$, as expected for a surface wave. As β is increased, the peak separation increases, either to reach a constant value of 60 mV at 20 °C for fast electron transfer ($\Lambda \rightarrow +\infty$) or to continue increasing with $\log(\beta)$ for finite values of Λ. Therefore, by measuring the variation of both the experimental peak current function and peak potentials upon increasing scan rate, one can in principle gain access to the value of both the rotational diffusion coefficient of the DNA rod, D_r, and the rate constant of the heterogeneous electron transfer between the electrode and the Fc head, k_s. In other words, the respective contribution of chain dynamics and of the rate of heterogeneous electron transfer to the kinetic control of the faradaic current can be discriminated by cyclic voltammetry. This represents a significant benefit as compared to the AC voltammetry techniques, commonly used in the literature to analyze the response of redox-DNA layers, which only yield an overall and unspecific first-order "electron transfer" rate constant from which the information regarding molecular motion and heterogeneous electron transfer cannot be separated.[8]

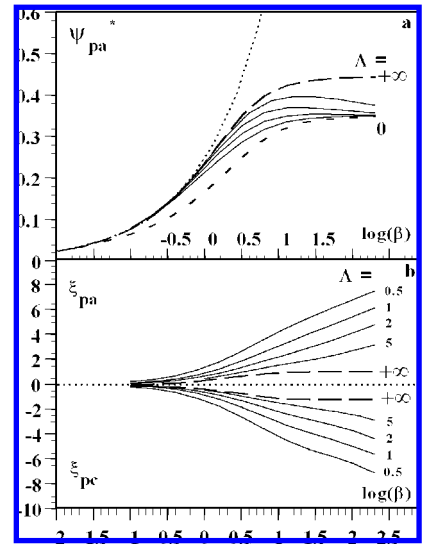

Figure 5. Variation as a function of $\log(\beta)$ of (a) the dimensionless peak current function (ψ^*_{pa}) and of (b) the dimensionless anodic (ξ_{pa}) and cathodic (ξ_{pc}) peak potentials of the voltammograms, calculated using the rotational diffusion model described in the text, for various values of Λ. In (a) the lower and upper dashed curves correspond respectively to an irreversible (slow, $\Lambda \rightarrow 0$) and to a Nernstian (fast, $\Lambda \rightarrow \infty$) electron transfer. The curves in continuous line correspond (from top to bottom) to $\Lambda = 5, 2, 1, 0.5$. In (b) the value of Λ is indicated near each curve. The dotted lines in (a) and (b) correspond to the characteristics of a surface-confined species (i.e. to a diffusionless system) displaying Nernstian electron transfer kinetics. $\beta = Fv/RTD_r$, $\Lambda = k_s/(D_rL)$, $\psi^*_{a,dif} = i_{pa}/FN_0(D_r)^{1/2}(Fv/RT)^{1/2}$, with v the can rate, D_r the rotational diffusion coefficient of the dsDNA rod, k_s the heterogeneous electron transfer rate constant and i_{pa} the anodic peak current. These graphs are the dimensionless equivalents of the experimental $i_{pa}/(\upsilon)^{1/2}$ and $E_{pa,c}$ vs $\log(\upsilon)$ plots.

5. Discussion

5.1. Cyclic Voltammetry Behavior of the Fc-dsDNA-C_6 Systems: General Conclusions. The voltammetric behavior of the Fc-dsDNA layers studied in the present work, and in particular the occurrence of a plateau in the current function, $i_{pa}/(\upsilon)^{1/2}$, vs $\log(\upsilon)$ plots (see Figures 2b and 4b), can be fully accounted for by the model presented above which describes the diffusional motion of the ferrocene head as resulting from the hinge movement of the dsDNA duplex. The DNA systems studied here (**I** and **II**) share the same relatively long C_6 surface linker but differ significantly from one another by the type and length of their Fc linkers (see Chart 1). Still, they display qualitatively similar voltammetric behaviors. Moreover, this behavior is in striking contrast with the one we previously reported for a dsDNA system consisting in a layer of end-grafted Fc-$[(dT)_{20}(dA)_{20}]$-C_2 chains **III**, for which a bell-shaped $i_{pa}/(\upsilon)^{1/2}$ vs $\log(\upsilon)$ variation was observed.[4] The latter variation was shown to reflect the fact that chain bending was controlling the dynamics of the C_2-end-grafted duplex **III**.

We attribute the difference between the dynamical behaviors of the end-anchored systems **I** and **II** on the one side and that of **III** on the other side to the fact that **III** was grafted on the surface very *directly* via a short C_2-linker, while the other systems are linked via a much longer C_6 linker. As a result, whereas free rotation of the dsDNA rod of **III** is largely hindered by sterical interactions between the surface and the lower part of the rod, such a hinge motion is possible for the dsDNA

systems anchored on the surface via longer linkers. In the "C_6" case simple rotation of the rod around its anchoring linker is sufficient for the Fc head to reach the electrode surface while in the "C_2" case bending of the dsDNA rod is required. Understandably free hinge motion of the rod is greatly facilitated if the length of the anchoring linker is close to, or larger than, the radius of the rod (~1 nm); such is the case for C_6-anchored systems, but not for C_2-anchored systems (length of the C_2 linker ~0.4 nm).

Therefore, what is originally demonstrated here is that the length of the surface linker of end-anchored dsDNA systems controls the type and geometry of the molecular motion of the dsDNA rod allowing the redox head to come into contact with the electrode. This result is expected to have important analytical implications since it is now increasingly recognized that the signaling mechanism of E-DNA sensors is based on the physical contact between the Fc head and the electrode surface, i.e. the so-called collisional mechanism.[8] This is particularly clear for those systems based on linear redox-DNA probes for which, as initially demonstrated by us,[4] and recently recalled by others,[9] hybridization detection is made possible by the difference in the *dynamical* behavior of end-anchored ss- and ds-chains. In this context it should be noted that, whereas for long surface linkers the faradaic current is controlled by an unspecific property of the duplex, i.e. its rotational diffusion, for short linkers it is controlled by an intrinsic property of the strand, i.e. its flexibility, which may be modulated by the presence of a mismatch or by the nucleotide sequence. Therefore using short rather than long surface linkers might result in an increased specificity of E-sensors for dsDNA detection.

More generally, all of the above illustrates the fact that cyclic voltammetry displays the unique benefit of allowing molecular motion to be unambiguously identified as contributing to the electrochemical response of redox-DNA layers. Moreover, the variation of the peak current function with scan rate provides a very clear and distinctive signature of the *type* of motion that the redox-dsDNA duplex undergoes to bring the Fc-head in contact with the electrode: a plateau-shaped variation is indicative of a purely diffusional motion while a peak-shaped variation indicates of an elastic bending motion of the duplex.

More quantitative conclusions regarding each of the DNA systems studied here are presented below.

5.2. Quantifying the Dynamics of the Hybridized Fc-DNA-C_6 Systems.

5.2.1. Perfectly Matched Grafted Duplexes Display Unexpectedly Slow Rotational Dynamics. For both of the Fc-DNA-C_6 systems **I** and **II**, and within the scan-rate range where a plateau is observed in the $i_{pa}/(\upsilon)^{1/2}$ vs $\log(\upsilon)$ plots, the peak-to-peak separation is observed to be close from ~60 mV, (see Figures 2 and 4). Consequently, the electron transfer can be considered as being Nernstian (i.e., fast) and the value of D_r, the rotational diffusion coefficient of the grafted DNA duplex, can be determined from the value of the plateau observed in the $i_{pa}/(\upsilon)^{1/2}$ vs $\log(\upsilon)$ variation, using eq 2 and $\psi_{pa,diff}* = 0.446$. This yields a value of $D_r = 2300\ (\pm 200)\ s^{-1}$ for the Fc-DNA-C_6 system **I**, and of $D_r = 200\ (\pm 50)\ s^{-1}$ for the Fc-DNA-C_6 system **II**. Both of these D_r values are spectacularly lower than the value of the rotational diffusion coefficient of a freely rotating ~20 mer DNA duplex, which is of $\sim 10^7\ s^{-1}$.[35] Slow apparent dynamics of nanometer-sized dsDNA strands, C_6-end-tethered to a gold surface, has already been reported but was attributed to instrumental limitations of the measuring technique.[36,37] In the present case, the very fact that undistorted voltammetric surface signals could be recorded for Fc-ssDNA at high scan rates, where the $i_{pa}/(\upsilon)^{1/2}$ vs $\log(\upsilon)$ variation for Fc-dsDNA was observed to reach a plateau, demonstrates that the slow dynamical behavior observed for the hybridized system is actual and does not arise from any response time limitation of our electrochemical setup. As a possible source of the observed slow dynamics of Fc-dsDNA-C_6 systems, the known slowing of the Brownian motion of a particle in the vicinity of a surface can be considered. However, for a rod-like particle the magnitude of this hydrodynamic effect is expected to be small, even for the worst case scenario of a rod diffusing perpendicularly to an interface.[38] Moreover, complete Brownian dynamic simulations of ~50 mer dsDNA end-anchored to a surface, taking into account hydrodynamic interactions and imposing a stringent no-slip boundary condition for the fluid field at the interface (zero fluid velocity at the anchoring surface), showed that the time scale of the duplex should still be in the order of a few tens of nanoseconds.[37] We attribute the apparent sluggishness of the rotational dynamics of C_6-anchored Fc-dsDNA to steric interactions occurring between the rotating rod and the surface, which hamper close approach of the rod from the electrode. According to this picture the rod would be freely diffusing from $\theta = 0$ to some limiting value of $\theta = \theta_i < \pi/2$, corresponding to the onset of repulsive DNA/surface interactions (Scheme 1). Diffusional motion of the rod from $\theta = \theta_i$ to $\theta = \pi/2$, or at least to an angle allowing the electron transfer to occur, would still be possible but significantly slowed since taking place in a repulsive force field. The diffusional field of the Fc head would still be hemispherical, and hence the rod would still appear to be moving as a result of free rotational diffusion, but much more slowly than expected. Since one can, *a priori*, envision that these Fc-DNA/surface interactions are electrostatic in nature, the role of electrostatic interactions in end-anchored DNA systems is worth discussing in detail here. It has been repeatedly reported in the literature that electrostatic interactions between the charged DNA helix and the double layer of the anchoring electrode determine the average orientation of end-anchored dsDNA chains, which consequently depends on the electrode potential.[39–41] Rant et al. have precisely quantified this orientating effect by measuring the ability of the electric field at the electrode to orientate short end-anchored dsDNA strands as a function of the supporting electrolyte concentration.[41] They observed that this ability is totally lost for electrolyte concentrations larger than 100 mM (see Figure 5a in ref 42), and concluded that electrostatic interactions between short DNA duplexes and the electrode surface are fully screened at high salt concentrations.

(35) Ortega, A.; García de la Torre, J. *J. Chem. Phys.* **2003**, *119*, 9914–9919.

(36) Rant, U.; Arinaga, K.; Tornow, M.; Kim, Y. W.; Netz, R. R.; Fujita, S.; Yokoyama, N.; Abstreiter, G. *Biophys. J.* **2006**, *90*, 3666–3671.

(37) Sendner, C.; Kim, Y. W.; Rant, U.; Arinaga, K.; Tornow, M.; Netz, R. R. *Phys. Status Solidi A* **2006**, *14*, 3476–3491.

(38) Trahan, J. F.; Hussey, R. G. *Phys. Fluids* **1985**, *28*, 2961–2967.

(39) (a) Kelley, S. O.; Barton, J. K.; Jackson, N. M.; McPherson, L. D.; Potter, A. B.; Spain, E. M.; Allen, M. J.; Hill, M. G. *Langmuir* **1998**, *24*, 6781–6784. (b) Zhou, D.; Sinniah, K.; Abell, C.; Rayment, T. *Langmuir* **2002**, *18*, 8278–8281. (c) Dong, L. Q.; Zhou, J. Z.; Wu, L. L.; Dong, P.; Lin, Z. H. *Chem. Phys. Lett.* **2002**, *354*, 458–465. (d) Zhang, Z.-L.; Pang, D.-W.; Zhang, R.-Y.; Yan, J.-W.; Mao, B.-W.; Qi, Y.-P. *Bioconjugate Chem.* **2002**, *13*, 104–109. (e) Ceres, D. M.; Barton, J. K. *J. Am. Chem. Soc.* **2003**, *125*, 14964–14965.

(40) Rant, U.; Arinaga, K.; Fujita, S.; Yokoyama, N.; Abstreiter, G.; Tornow, M. *Nano Lett.* **2004**, *4*, 2441–2445.

(41) Rant, U.; Arinaga, K.; Fujita, S.; Yokoyama, N.; Abstreiter, G.; Tornow, M. *Org. Biomol. Chem.* **2006**, *4*, 3448–3455.

Considering the fact that the experiments reported here are conducted using 1 M $NaClO_4$ as supporting electrolyte one can therefore safely conclude that the orientation of the end-anchored Fc-dsDNA is not dependent on the electrode potential, but is solely determined by random thermal motion.

Moreover, Rant et al.[41] also demonstrated that, for such a high ionic strength, even for the worst case scenario of a *negatively* biased electrode, the repulsive electrostatic energy between a flat-lying dsDNA rod and the electrode is barely above thermal energy (see Figure 6 in ref 42). This means that double-layer forces are not sufficient to effectively oppose close approach of the dsDNA rod to the electrode surface down to $\theta = \pi/2$.

It is, however, noteworthy that, in experiments involving electrical manipulation of short dsDNA strands, orientating the dsDNA duplex at an angle greater than 55° from the surface normal was observed to be unexpectedly difficult, plausibly as a result of DNA/surface steric hindrance.[41] AFM/SECM experiments are currently conducted to explore this possibility and to identify the exact nature of the postulated rod/surface repulsive interactions.

Interestingly, in spite of these DNA/surface interactions, the Fc head can approach the electrode surface closely enough for the electron transfer not only to take place but also to be fast enough so as to appear Nernstian. However, this simply requires that $\Lambda = k_s/(D_r L) \gg 1$, i.e. that the rate constant for the heterogeneous electron transfer between the Fc head borne by the duplex and the electrode surface is such that: $k_s \gg 2 \times 10^{-3}$ cm/s and $k_s \gg 2 \times 10^{-4}$ cm/s, respectively for the Fc-DNA-C_6 systems **I** and **II**.

5.2.2. Comparison of Fc-DNA Systems I and II: Effect of the Fc Linker Effect. Considering the chemical structures of **I** and **II**, the 1 order of magnitude difference in the D_r values derived for the Fc-DNA-C_6 systems **I** and **II** can only be due to the markedly different Fc linker of the two strands. As seen in Chart 1, the Fc head in **I** is attached to the uracil base via a relatively rigid linker (~1 nm long), while the Fc head in **II** is connected to the 3′-phosphate group via a 11 σ-bond long linker, including a six-carbon-atom long alkyl chain (~1.4 nm in length). It seems reasonable to assume that, in the highly ionic aqueous environment used here, the hydrophobic alkyl linker of **II** is coiled which renders the Fc head probably less accessible to the electrode in Fc-dsDNA **II** than in Fc-dsDNA **I**. As a result a closer approach of the rod from the surface is required for the electron transfer to take place, which is made unfavorable by repulsive dsDNA/surface interactions, and translates into a lower apparent rotational diffusion coefficient for dsDNA **II** than for **I**. Interestingly and in spite of that, the electron transfer still appears Nernstian for the duplex of **II**, i.e. the rate of heterogeneous electron transfer at the electrode does not appear to be significantly slower for dsDNA **II** than for dsDNA **I**. As seen from the definition of $\Lambda = k_s/(D_r L)$, this simply reflects the fact that D_r and k_s control the apparent electron transfer kinetics in an exact opposite way: a lowering of D_r can compensate and mask any lowering of k_s as long as the D_r/k_s ratio remains unchanged. We also note that the overall apparent dynamics of **II** is comparable *in magnitude* to the one observed for **III**, as suggested from the similar intensity of the $i_{pa}/(v)^{1/2}$ vs log (v) plots obtained in both cases (compare dashed and continuous lines in Figure 4b). This indicates that going from a "C_2"- to a "C_6"-anchored dsDNA system, while keeping comparable Fc linkers (i.e., from **II** to **III**), changes the type of motion of the duplex but has little effect on the overall apparent dynamics.

5.2.3. Electron Transport by Molecular Motion of dsDNA Is Faster than DNA CT. An important result of our work is that the voltammetric response of all of the Fc-dsDNA systems **I**, **II**, and **III** that we've studied so far can be fully accounted for by considering molecular motion of the dsDNA rod as the *sole* electron transport process. Consequently, it can be concluded that electron transport through the dsDNA duplex (DNA CT) is not playing any role for these systems. This result falls in line with recent reports showing that electronic coupling of the redox probe with the DNA base stack is a prerequisite for the occurrence of DNA CT, such a coupling being realized by linking the redox probe to the terminal base of the target DNA strand via an unsaturated acetylene linker.[5,6] In these reports, charge transport by molecular motion of the whole DNA rod was considered to occur *only* in the absence of such a coupling, i.e. when an alkyl-linked probe was used.[5] It should, however, be recalled that Brownian motion of the redox-dsDNA strand is a universal charge transport mechanism which will unavoidably compete *kinetically* with DNA CT, independently of the type of probe and linker used. In that context we note that DNA CT through C_6-anchored dsDNA chains was reported to take place with a characteristic rate constant of ~90 s^{-1},[42] which is lower than the D_r values we measured here for the double-stranded Fc-DNA-C_6 systems. This result demonstrates that charge transport by simple rotational motion of the C_6-anchored dsDNA rod can actually compete *favorably* with DNA CT and should therefore be considered even for those systems where DNA CT is possible.

Understandably, for such systems, experimental conditions that would tend to slow the dynamics of the dsDNA rod, or hamper close approach of the rod from the surface, would increase the relative contribution of DNA CT to the overall electron transport within the dsDNA layer. Among these conditions one can envision the use of a very high DNA coverage, which favors steric interactions between neighboring dsDNA chains, or of a low salt concentration, which may result in dsDNA/electrode repulsive interactions, depending on the potential region explored.[39–41]

6. Conclusion

The cyclic voltammetry behavior of molecular layers of 3′-ferrocenylated $(dT)_{20}$ (or $ddU(dT)_{19}$) strands, 5′-end-grafted onto a gold electrode surface via a long C_6 linker has been studied. Single-stranded Fc-DNA layers were observed to behave as diffusionless systems reflecting the rapid dynamics of the ssDNA strand. Following hybridization, the Fc-dsDNA layers gave rise to a yet unreported cyclic voltammetry behavior characterized by a sigmoid-shaped variation of the current function with scan rate. This variation provides evidence that the Fc-head is animated by a purely diffusional motion, ascribed to free rotation of the rigid DNA duplex around its C_6 anchoring linker. This result contrasts with the behavior we previously reported for a layer of Fc-dsDNA chains grafted on gold surfaces via a short C_2-linker, and for which the motion of the Fc head was shown to result from elastic bending of the duplex.

We therefore demonstrated here that the length of the surface linker determines the *type o*f molecular motion undergone by

(42) Kelley, S. O.; Barton, J. K.; Jackson, N. M.; Hill, M. G. *Bioconjugate Chem.* **1997**, *8*, 31–37.

end-grafted Fc-dsDNA rods allowing the Fc head to contact the electrode surface. Long surface linkers allow simple free hinge motion of the duplex, while this motion is sterically hindered if short surface linkers are used, and bending of the dsDNA rod is in that case required for the electron transfer to take place.

An appropriate model, describing the motion of the dsDNA-borne Fc head as resulting from hinge motion of the DNA duplex, allowed us to quantify the molecular dynamics of the C_6-anchored Fc-dsDNA chains in terms of an apparent rotational diffusion coefficient, D_r. The value found for D_r was $\sim 3-4$ orders of magnitude slower than expected for the rotation of free dsDNA in solution, pointing to a drastic motion-slowing role of the anchoring surface. We postulate that repulsive dsDNA rod/surface interactions are responsible for such an unreported phenomenon of slowed diffusion of end-anchored dsDNA in the immediate vicinity of the bearing electrode surface. Comparing the D_r values we obtained for two C_6-anchored Fc-dsDNA systems, differing by the chemical structure and length of the linker connecting the Fc head to the probe DNA strand, allowed us to show that the accessibility of the Fc head for the electron transfer at the electrode largely modulates the *apparent dynamics* of the DNA rod. Importantly, this effect cannot result from a modulation of the rate of the heterogeneous electron transfer to the Fc head. It rather arises from the fact that, in the case of a poorly accessible Fc head, a closer approach of the DNA duplex from the repelling electrode surface is required for the electron transfer to take place.

The dynamics of Fc-dsDNA was found to be insensitive to the presence of a single mismatch in the middle of the strand, demonstrating that charge transport by conduction along the dsDNA helix (DNA CT) is not present for the systems studied here. However in any case, electron transport by simple hinge motion of the dsDNA chain was found to be fast enough to, *a priori*, compete kinetically favorably with DNA CT and should therefore be considered even for the systems where charge transport by DNA CT was evidenced.

This work is also a clear demonstration that cyclic voltammetry is a very powerful tool to elucidate the signaling mechanism of conformation-linked DNA electrochemical biosensors, particularly because this technique uniquely allows DNA molecular motion to be unambiguously identified as contributing to the electrochemical signal.

JA801074M